Limited net role for climate change in heavy spring rainfall in Emilia-Romagna

1. Clair Barnes, Grantham Institute, Imperial College London, UK
2. Davide Faranda, Laboratoire des Sciences du Climat et de l'Environnement, CEA - CNRS - UVSQ, Université Paris-Saclay, IPSL, Gif-sur-Yvette, France & London Mathematical Laboratory, London, UK
3. Erika Coppola, *Abdus Salam International Centre for Theoretical Physics, Trieste, Italy*
4. Federico Grazzini, *Ludwig-Maximilians-Universität, Meteorologisches Institut, München, Germany & ARPAE-SIMC, Regione Emilia-Romagna, Bologna, Italy*
5. Mariam Zachariah, *Grantham Institute, Imperial College, London, UK*
6. Chen Lu, *Abdus Salam International Centre for Theoretical Physics, Trieste, Italy*
7. Joyce Kimutai, *Grantham Institute, Imperial College London, UK*
8. Izidine Pinto, *Royal Netherlands Meteorological Institute (KNMI), De Bilt, The Netherlands*
9. Carolina Marghidan Pereira, *Red Cross Red Crescent Climate Centre, The Hague, the Netherlands*
10. Sayanti Sengupta, *Red Cross Red Crescent Climate Centre, The Hague, the Netherlands*
11. Maja Vahlberg, *Red Cross Red Crescent Climate Centre, The Hague, the Netherlands*
12. Roop Singh, *Red Cross Red Crescent Climate Centre, The Hague, the Netherlands*
13. Dorothy Heinrich, *Red Cross Red Crescent Climate Centre, The Hague, the Netherlands*
14. Friederike E. L. Otto, *Grantham Institute, Imperial College London, UK*

Main findings

- While the full profile of the impacts on human life and livelihoods has yet to be analysed, initial assessments show that the floods and landslides caused 17 fatalities and displaced roughly 50.000 people. The majority of the deceased were elderly and died in their homes, in many cases linked to either reduced mobility or reluctance to evacuate. These deaths highlight how pre-existing vulnerabilities such as disability and limited risk perception exacerbated the impacts in the region.
- For observational analysis, we looked at spring rainfall in the study region based on a dense network of about 60 weather stations in the area that have consistent data since at least the 1960s. The heavy rainfall over the first 21 days of May 2023 is the wettest event of this type in the record with a return time estimated to be about 200 years. This means that in any given year, the chance of such an event occurring is about 0.5%.
- In the station data as well as other observational data products there is no significant trend in the 21-day spring rainfall: thus the amount of rain that falls in a 200-year event today is the same as in a 200-year event at the beginning of the record.
- To determine whether there is indeed no trend due to human-induced climate change or whether a trend is masked by changes in other drivers of rainfall, such as land-use changes or changes in aerosols, we look at the same 21-day event in climate models with and without the human-

https://doi.org/10.25561/104550.

induced increase in climate change. Of the 19 models used, none of them show a significant change in the likelihood or intensity of such an event to occur. This suggests that in contrast to most parts of the world, there is indeed no detectable increase in heavy rainfall in the Emilia-Romagna region in spring.

- This finding corroborates earlier research that has found that with human-induced climate change the number of low-pressure systems in the central Mediterranean has decreased. This leads to a reduction in heavy rainfall, offsetting the expected increase in heavy rain from global warming.
- In recent decades, rapid urbanisation and increasingly dense urban fabric has limited space for water drainage and increased risk of flooding, which has exacerbated the impacts of the heavy rainfall. However, this was an extremely rare event, and most infrastructure cannot reasonably be built to withstand such low-frequency events.
- There are many adaptation options that are robust to multiple types of extremes (e.g. drought, heat, floods) and also have co-benefits for societal well-being and biodiversity, which can increase the resilience of this region to future extremes. Nature-based solutions, social protection, and improved urban planning, are just a few examples.

1 Introduction

During the month of May 2023 the North Italian region of Emilia-Romagna (ER), particularly the provinces of Bologna, Ravenna, Forlì-Cesena, Rimini, experienced severe flooding, following three separate heavy rainfall events on the 2nd, 10th, and 16th of May. In the first week of May, the region of Emilia-Romagna received torrential rain for 48 hours (2-3 May) leading to flooding and landslides (ANSA, 4 May 2023). The province of Bologna recorded around 190mm of precipitation in less than 48 hours. Other affected areas in Emilia-Romagna include Ravenna and Forlì-Cesena provinces (Floodlist, 4 May 2023). Water level in the Lamone river rose by 10m in less than 24 hours (Floodlist, 4 May 2023) and an embankment along the Lamone River failed in Faenza, in the province of Ravenna, flooding the city. The associated impacts to lives and infrastructure led to the declaration of a state of emergency for the region (ANSA, 4 May 2023). After this first spell, the region again received heavy downpours during the second week of May, and then again in the third week starting on 16th May, with another event of heavy precipitation of the same magnitude as the one observed at the beginning of the month. In total six months' worth of rain fell in the first 20 days of May (euronews.green, 22 May 2023). This second event resulted in 23 river banks being flooded in the region, submerging settlements, leaving thousands homeless and killing at least 15 people (The Guardian, 17 May 2023; ANSA 20 May 2023).

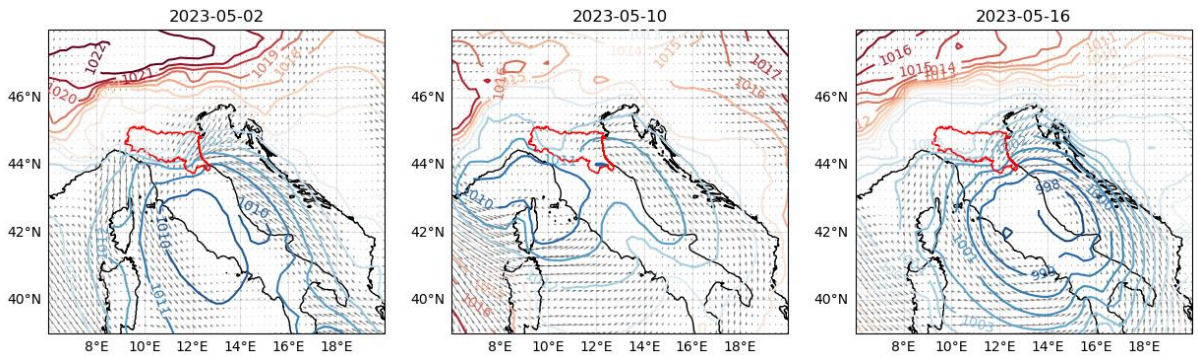

https://doi.org/10.25561/104550.

***Figure 1**: Synoptic conditions over Italy (taken from ERA5 reanalysis) on May 2nd, 10th and 16th. Contours indicate daily mean sea level pressure [hPa] and arrows indicate the prevailing wind direction, with longer arrows denoting higher wind speeds. The Emilia-Romagna region is outlined in red.*

All three rainfall events were driven by three distinct low-pressure systems, situated over the Tyrrhenian Sea (Figure 1). A very high and anomalous water vapor transport from south-east at mid-level was associated with the last cyclone. The interaction between these cyclonic systems and the low level northeasterly (NE) wind along the Adriatic side of the Apennines generated a meteorological phenomenon called “stau” or “orographic lifting”. This process occurs when the NE wind encounters the mountain range, causing it to ascend and cool as it rises over the higher elevations. As the air ascends, it undergoes adiabatic cooling, leading to condensation and cloud formation. Consequently, precipitation is enhanced on the windward side of the mountains which, in this case, are the eastern slopes of the Apennines facing the Adriatic Sea. The orographic lifting of moist NE winds over an extended period can result in persistent and heavy rainfall on the eastern slopes of the Apennines. With prolonged rainfall, the soil becomes saturated, and the excess water runs off more quickly into rivers and streams, increasing river levels and contributing to the risk of flooding. The prolonged advection of moisture by NE winds can also enhance the runoff by continuously supplying moisture to the eastern side of the mountains. The prolonged stau effect can contribute to significant water accumulation, potentially overwhelming drainage systems, exceeding riverbanks' capacity and resulting in flooding along the watercourses. In areas with steep terrain and narrow valleys, the combination of prolonged heavy rainfall and enhanced runoff can lead to flash floods as the excess water accumulates rapidly, causing sudden and potentially dangerous flooding in these localised areas. Finally, it is important to note that the specific impacts of flooding during a prolonged cyclonic event can vary based on factors such as the intensity and duration of the rainfall, the topography of the affected areas, and the capacity of local drainage systems. Additionally, the condition and management of river systems can influence the extent of flooding.

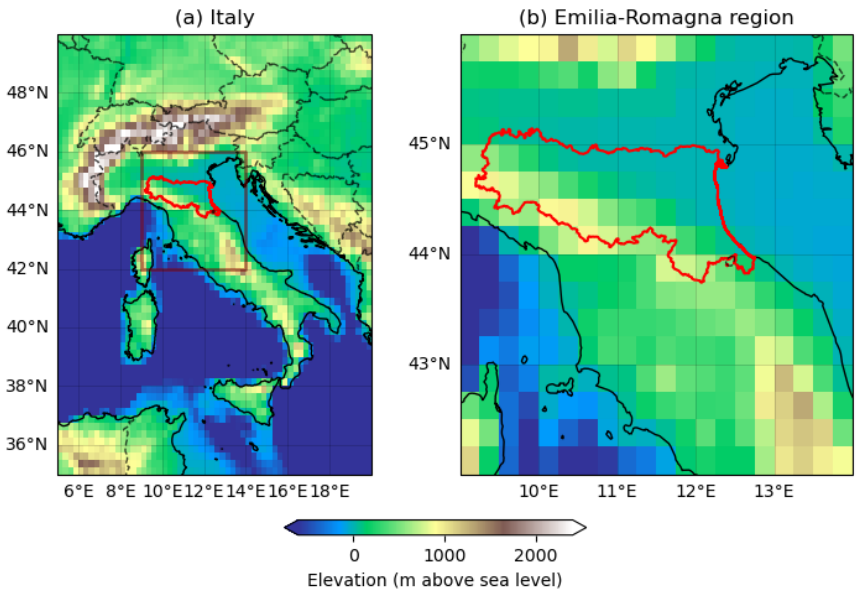

***Figure 2**: Elevation map of (a) Italy and (b) the region bounded by the shaded box in (a), with the Emilia-Romagna region outlined in red.*

https://doi.org/10.25561/104550.

According to local experts, the timing of these heavy rainfall episodes in the ER region also contributed to the exceptional nature of the impacts. Northern Italy had been under drought during the last two years due to below-average snowfall in the Alps, Dolomites and Apennines in the winter affecting snowmelt that contribute steady runoff to the region's water bodies (VOA, 21 May 2023). The heavy rainfall during May 2-3 fell on dry and impermeable ground causing the water to wash over the topsoil out into the sea (The Guardian, 19 May 2023). As a result of this heavy precipitation the ground rapidly became saturated, increasing the runoff and thus the severity of the flooding during the subsequent events.

The ER region, located between the Apennine mountains and the Adriatic, has seen many severe flood events in the past, most of which occurred in the autumn or winter months. Notably in the Autumn 1963 landslides and floods occurred in Romagna and Emilia due to torrential rains. In the province of Forlì, collapses occurred in Bagno di Romagna, Civitella Romagna (2 landslides), Predappio (5 landslides), Premilcuore, Santa Sofia, Sarsina, Torriana, and Verghereto. In the province of Ravenna, landslides occurred in Brisighella, including 11 landslides, one of which overwhelmed the church and rectory of Monticino and brushed against the centre of Brisighella. Collapses also occurred in Casola (7 landslides) and Riolo Terme (4 landslides). The landslides in Romagna during those days covered approximately 1,700 hectares in total. Another devastating year was 1973 where from January 1 to October dozens of floods occurred throughout the region. On March 7 and 8, 1973, in Ravenna, the network of ditches failed to drain the water, resulting in the flooding of 20 square kilometres of city and countryside. On September 27, 1973, the Pisciarello stream flooded the fields between Ponte Pietra and Casone, interrupting the state road 304 in Cesena. Two further notable floods in the spring occurred in 1978, in Brisighella (Ravenna) in the Zattaglia area, and in March 1985, when spring rains set the Case Gamberini landslide in motion in Bagno di Romagna, near the course of the Savio River. However none of these singular events are close by extension and severity to the one which occurred in May 2023. The closest similar event is the one that happened in May 1939 when many rivers in Romagna flooded and there were many landslides in the hills (Annale Idrologico 1939, Parte 2, Ministero Lavori Pubblici, Servizio Idrografico, (Italian)).

The larger Mediterranean region of which Italy and the ER region are part is one of the few regions in the world where there are many studies and abundant high-quality data, but no discernible trends in heavy precipitation (Seneviratne et al, 2021). The hydrological cycle of the Mediterranean region is known to be affected by global warming; however, assessments of the effects on extreme precipitation remain uncertain due to high natural variability and contrasting thermodynamic and dynamical trends acting on the region (Pfahl et al, 2017). The overall trend is for a significant increase in drought but changes in seasonality may lead to less frequent but more intense heavy rain events, mostly concentrated in autumn and progressively moving also into the cold season (Persiano et al. 2022, Pavan et al. 2019). This means that the compounding conditions which exacerbated the impacts of this event, with heavy rainfall falling on very dry soils leading to particularly rapid run-off and flash flooding (typical of autumn), are expected to be more frequent in the future.

The flooding in May 2023 was linked to three distinct low pressure systems identified as Mediterranean cyclones. Emerging research has highlighted a concerning decline in rainfall due to both the diminishing strength of such cyclones (Flaounas et al., 2022) and their decreasing occurrence. These trends, already apparent in the current climate, are anticipated to persist under scenarios of anthropogenic global warming (Reale et al., 2022), although the certainty surrounding these changes is limited due to considerable variations among models in representing these phenomena.

https://doi.org/10.25561/104550.

Given that the deluge and the impacts over the Emilia-Romagna (henceforth ER) region were a consequence of a series of short but heavy rainfall spells occurring within a span of three weeks, we define the event for the remainder of the study as the maximum accumulated 21-day rainfall (Rx21d) in April-June (AMJ), averaged over the ER region. Fig. 3 shows the 21-day accumulated precipitation from May 1-21, 2023 over Emilia-Romagna (42-46ºN 9-14ºE). The study domain is outlined in red.

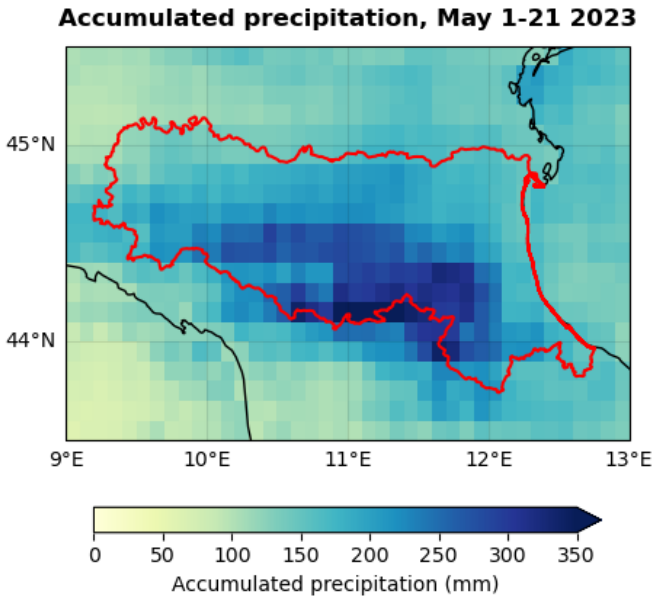

Figure 3: *21-day accumulated precipitation from May 1st-21st, the wettest three-week period in 2023 in the Emilia-Romagna region (outlined in red). Data are from MSWEP.*

2 Data and methods

2.1 Observational data

We use three independent gridded data products to analyse the rainfall in the study region.

1. Station-based composite: The station-based observed daily precipitation is aggregated from two datasets. One is SCIA (Sistema nazionale per la raccolta, l'elaborazione e la diffusione di dati Climatologici di Interesse Ambientale) constructed by ISPRA (Istituto superiore per la protezione e la ricerca ambientale), which covers the record from 1960 to 2021. The other dataset is ARPAE (L'Agenzia regionale per la prevenzione, l'ambiente e l'energia dell'Emilia-Romagna, data available at: https://simc.arpae.it/dext3r/), which is used to extend the record to May 24, 2023. Stations were selected for inclusion in the composite if at least 40 years of data was available, with a maximum of 20% missing values in any given year. After applying these criteria, 60 stations were used to create the composite (Figure 4).
2. MSWEP: The Multi-Source Weighted-Ensemble Precipitation (MSWEP) v2.8 dataset (updated from Beck et al., 2019) is fully global, available at 3-hourly intervals and at 0.1° spatial resolution, available from 1979 to ~3 hours from real-time. This product combines gauge-, satellite-, and reanalysis-based data for reliable precipitation estimates.
3. ERA5: We use daily precipitation data from the ERA5 reanalysis product (Hersbach et al., 2020), which is available at 0.25° spatial resolution from 1950 onwards. It should be noted that

the variables from ERA5 are not directly assimilated, but are generated by atmospheric components of the European Centre for Medium-Range Weather Forecasts' Integrated Forecast System.

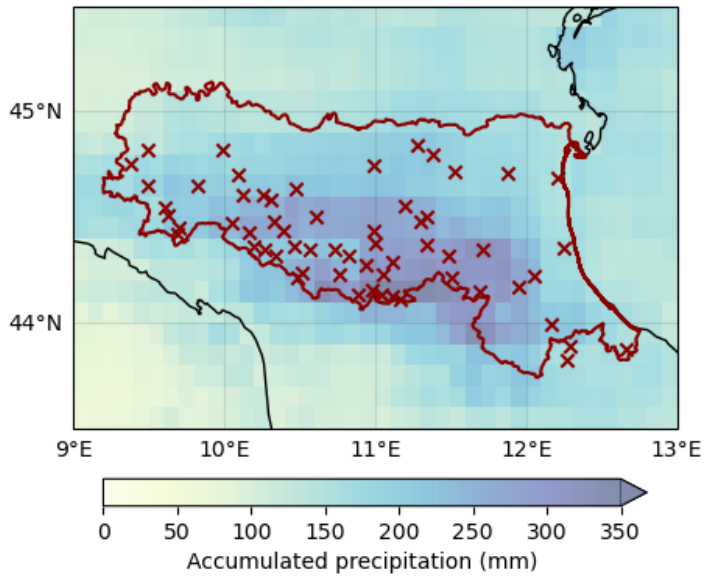

Figure 4*: Location (dark red crosses) of 60 stations used to produce the composite time series, plotted over the accumulated precipitation from May 1st-21st 2023 (MSWEP). The Emilia-Romagna region is outlined in dark red.*

As a proxy for anthropogenic climate change we use the (low-pass filtered) global mean surface temperature (GMST) anomalies with respect to 1951-1980, where GMST is taken from the National Aeronautics and Space Administration (NASA) Goddard Institute for Space Science (GISS) surface temperature analysis (GISTEMP, Hansen et al., 2010 and Lenssen et al. 2019).

2.2 Model and experiment descriptions

We use three multi-model ensembles from climate modelling experiments using very different framings (Philip et al., 2020): Sea Surface temperature (SST) driven global circulation high resolution models, and regional climate models.

1. Coordinated Regional Climate Downscaling Experiment (CORDEX) - European Domain with 0.11° resolution (EUR-11) (Jacob et al., 2014; Vautard et al., 2021; Coppola et al., 2021). The ensemble used here consists of 59 simulations produced by combinations of six Global Climate Models (GCMs) and eleven Regional Climate Models (RCMs). These simulations are driven by historical forcings up to 2005, and extended to the year 2100 using the RCP8.5 scenario.

2. UKCP18 land-RCM: This is a twelve-member perturbed physics ensemble developed by the UK Met Office (Murphy et al., 2018). The ensemble members are derived from HadGEM3-GC3.05, a high-resolution (about 60km) coupled ocean-atmosphere model, dynamically downscaled to a resolution of 0.11° (about 12km) over Europe using HadREM3-GA7-05. Each ensemble member uses the same perturbations at both 60km and 12km resolutions, and the members additionally sample a range of future emissions consistent with the RCP8.5 pathway (Sexton et al., 2021).

https://doi.org/10.25561/104550.

3. HighResMIP SST-forced model ensemble (Haarsma et al. 2016), the simulations for which span from 1950 to 2050. The SST and sea ice forcings for the period 1950-2014 are obtained from the 0.25° x 0.25° Hadley Centre Global Sea Ice and Sea Surface Temperature dataset that have undergone area-weighted regridding to match the climate model resolution (see Table B). For the 'future' time period (2015-2050), SST/sea-ice data are derived from RCP8.5 (CMIP5) data, and combined with greenhouse gas forcings from SSP5-8.5 (CMIP6) simulations (see Section 3.3 of Haarsma et al. 2016 for further details). Four HighResMIP models were used in this study.

2.3 Statistical methods

In this analysis we examine annual time series of maximum 21-day accumulated rainfall (Rx21d) for the AMJ season, averaged over the Emilia-Romagna (ER) region, using the longest available records of observed and reanalysis data. Methods for observational and model analysis and for model evaluation and synthesis are used according to the World Weather Attribution Protocol, described in Philip et al. (2020), with supporting details found in van Oldenborgh et al. (2021), Ciavarella et al. (2021) and here.

The analysis steps include: (i) trend calculation from observations; (ii) model evaluation; (iii) multi-method multi-model attribution and (iv) synthesis of the attribution statement.
We calculate the return periods, Probability Ratio (PR; the factor-change in the event's probability) and change in intensity of the event under study, in order to compare the climate of now and the climate of the past, defined respectively by the GMST values of now and of the preindustrial past (1850-1900, based on the Global Warming Index). To statistically model the event under study, we use a GEV distribution that scales with GMST, with the dispersion (the ratio of the variance to the mean) kept constant. Next, results from observations and models that pass the evaluation tests are synthesised into a single attribution statement.

3 Observational analysis: return period and trend

Figure 5 shows the time series of maximum 21-day accumulated precipitation in the AMJ season averaged over ER along with the 10-year running averages (shown by the smooth red lines) , based on (a) composite from stations, (b) MSWEP and (c) ERA5. There is no discernible trend in Rx21d in the station composite or the gridded datasets, and the extreme precipitation during this year is captured in all products.

https://doi.org/10.25561/104550.

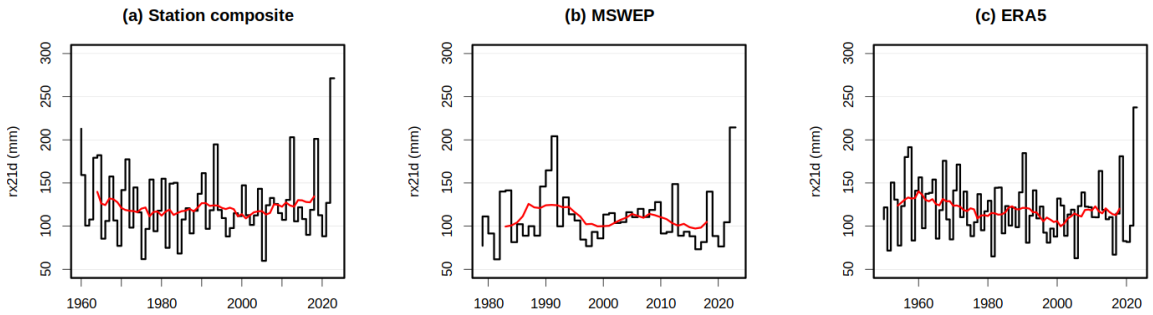

Figure 5: *Time series of AMJ maxima of 21-day accumulated rainfall along with the ten-year running mean (shown by red line) for ER based on (a) station composites (b) MSWEP and (c) ERA5 datasets.*

Figure 6 shows the results of the trend fitting methods described in Philip et al. (2020) applied to the maximum 21-day accumulated rainfall in the AMJ season, averaged over the ER region based on (a) station composites, (b) MSWEP and (c) ERA5 datasets. The left-hand panels show the variable as a function of the GMST anomaly, while the right-hand panels show the GEV return period curves for this variable in the 2023 climate (red lines) and in a 1.2°C cooler climate (blue lines). In the composite and MSWEP, there is almost no trend in Rx21d with GMST: the longer ERA5 dataset shows a slight downward trend, but this is not statistically significant. The return period of the 2023 event is close to 200 years in the station composite (uncertainty: 36 years to infinite) and MSWEP (uncertainty: 20 to 40,500 years); and around 400 years (uncertainty: 60 years to infinite) in ERA5. For the attribution analysis, we define the 2023 event as a 1-in-200 year event. The Probability Ratio (PR) is close to 1 (with large uncertainties encompassing no change) in the station composite and MSWEP datasets, reflecting the absence of evidence of climate change in the 2023 event. The best estimate for PR is lower in ERA5, about 0.4; again, this is not significant, with large uncertainty (0-6). Consequently the change in intensity between the 2023 climate and a 1.2°C cooler climate is also very small in these datasets, with large uncertainties: 4% increase in the station composites (uncertainty: -49% to 30%), 3% decrease in MSWEP (uncertainty: -32% to 40%) and 10% decrease in ERA5 (uncertainty: -28% to 16%).

https://doi.org/10.25561/104550.

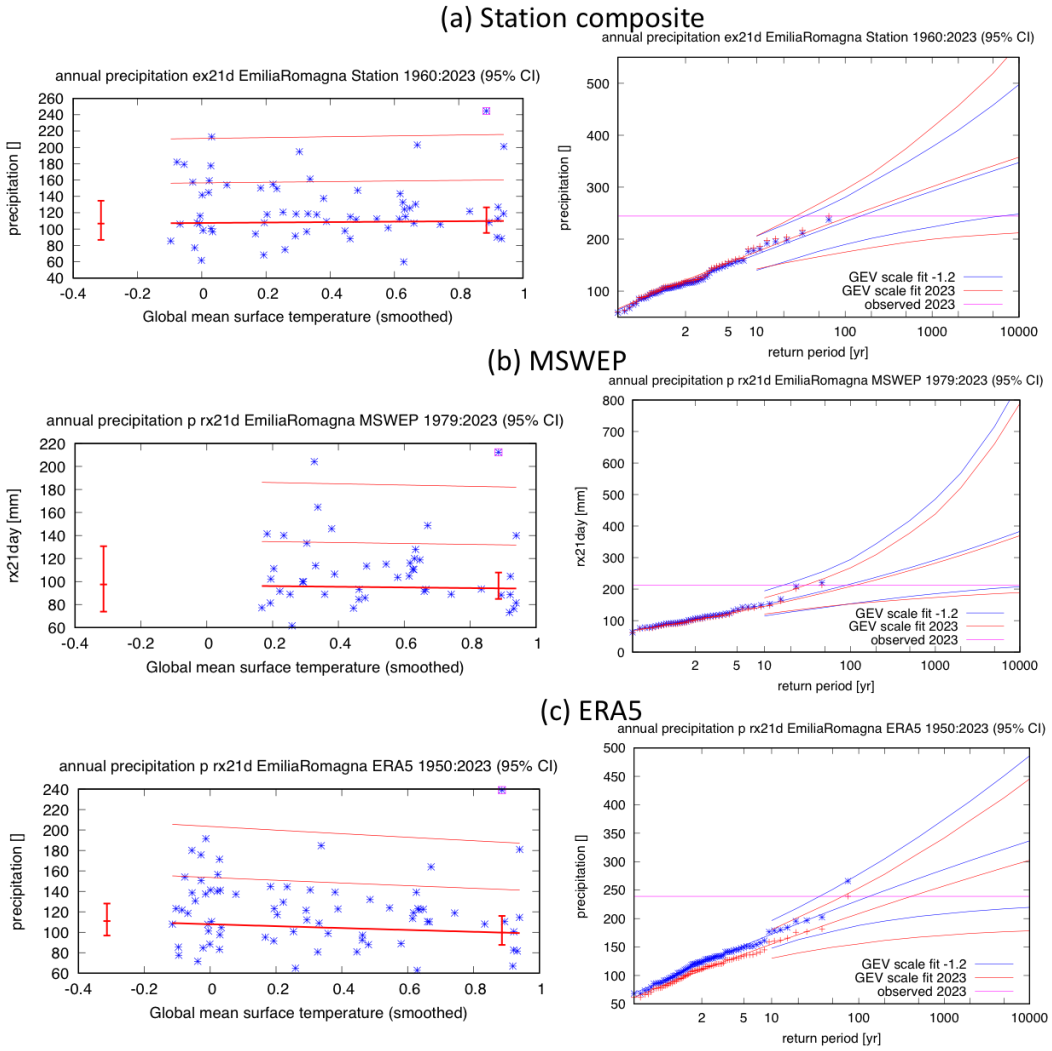

Figure 6: *GEV fit with constant dispersion parameter, and location parameter scaled proportional to observed GMST, for the ER region based on (a) station composites (b) MSWEP and (c) ERA5. The 2023 event is included in the fit.* ***Left****: Observed AMJ Rx21d as a function of the smoothed GMST. The thick red line denotes the time-varying location parameter; the thinner lines above indicate 6-year and 40-year effective return levels. The vertical red lines show the 95% confidence interval for the location parameter for the 2023 climate and a 1.2ºC cooler climate. The 2023 observation is highlighted with the magenta box.* ***Right****: Return time plots for the climate of 2023 (red) and a climate with GMST 1.2 ºC cooler (blue). The past observations are shown twice: once shifted up to the current climate and once shifted down to the climate of the late nineteenth century. The markers show the data and the lines show the fits and uncertainty from the bootstrap. The magenta line shows the magnitude of the 2023 event.*

4 Model evaluation

In the subsections below we show the results of the model evaluation for the AMJ Rx21d, for the ER region (Table 1). The evaluation period considered is 1979-2023, the period covered by all three observational data products. If five models or fewer perform well for a particular model setup, we include models that only just pass the evaluation tests for that model setup. The climate models are evaluated against the observations in their ability to capture:

https://doi.org/10.25561/104550.

1. Seasonal cycles: For this, we qualitatively compare the seasonal cycle of daily precipitation in ER in the climate model outputs against the cycle computed from MSWEP. We discard any models that exhibit ill-defined peaks in their seasonal cycles.

2. Spatial patterns: Models that do not match the observations in terms of the large-scale pattern of mean precipitation during May are excluded.

3. Parameters of the fitted GEV model: We discard the model if the 95% confidence intervals of the shape and dispersion parameters of the fitted GEV do not overlap with those estimated from the gridded observations.

The models are classified as 'good', 'reasonable', or 'bad' based on their performance in each of the three criteria discussed above. If the model is 'good' for all of these criteria, we give it an overall rating of 'good' (green highlight). We rate the model as 'reasonable' or 'bad', if it is rated 'reasonable' or 'bad', respectively, for at least one of the three criteria. These are respectively shown by the yellow and red highlights in the tables below. Where multiple realisations of the same GCM-RCM pairing in the EuroCORDEX ensemble pass validation, only one is selected for inclusion in the final analysis. Nine EuroCORDEX and five UKCP18 runs were classified as 'good'; five additional 'reasonable' UKCP18 runs were also included in the analysis.

Table 1: *Evaluation results for the climate models considered for the attribution analysis of AMJ maxima of 21-day accumulated rainfall of 2023 area-averaged over the ER region. The table contains qualitative assessments of seasonal cycle and spatial pattern of precipitation from the models (good, reasonable, bad) along with estimates for dispersion parameter, shape parameter and event magnitude. The corresponding estimates for observations are shown in blue. Based on overall suitability, the models are classified as good, reasonable and bad, shown by green, yellow and red highlights, respectively.*

Model / Observations	**Seasonal cycle**	**Spatial pattern**	**Dispersion**	**Shape parameter**	**Event magnitude (mm)**
Station composite			0.275 (0.207 ... 0.328)	-0.0021 (-0.15 ... 0.17)	271.33
MSWEP			0.221 (0.147 ... 0.267)	0.096 (-0.10 ... 0.50)	214.38
ERA5			0.256 (0.209 ... 0.292)	-0.040 (-0.18 ... 0.11)	237.56
					Threshold for 200-yr return period
CORDEX					
CNRM-CM5_r1_ALADIN53 (1)	bad	reasonable	0.221 (0.156 ... 0.268)	-0.099 (-1.0 ... 0.061)	275.074
CNRM-CM5_r1_ALADIN63 (1)	good	good	0.224 (0.152 ... 0.269)	-0.088 (-0.68 ... 0.15)	265.156

https://doi.org/10.25561/104550.

CNRM-CM5_r1_ALARO-0 (1)	good	good	0.226 (0.150 ... 0.280)	-0.12 (-0.42 ... 0.18)	240.510
CNRM-CM5_r1_CCLM4-8-17 (1)	reasonable	good	0.270 (0.187 ... 0.342)	-0.16 (-0.90 ... 0.084)	243.011
CNRM-CM5_r1_crCLIM-v1-1 (1)	bad	good	0.242 (0.185 ... 0.290)	-0.038 (-0.49 ... 0.29)	207.821
CNRM-CM5_r1_HadREM3-GA7-05 (1)	good	good	0.327 (0.233 ... 0.396)	-0.33 (-0.99 ... 0.080)	219.635
CNRM-CM5_r1_RACMO22E (1)	reasonable	good	0.316 (0.227 ... 0.385)	-0.23 (-0.64 ... -0.071)	239.417
CNRM-CM5_r1_RCA4 (1)	good	reasonable	0.291 (0.217 ... 0.353)	-0.14 (-0.52 ... 0.064)	225.220
CNRM-CM5_r1_RegCM4-6 (1)	bad	reasonable	0.232 (0.149 ... 0.304)	-0.41 (-1.0 ... 0.15)	171.093
CNRM-CM5_r1_REMO2015 (1)	bad	good	0.223 (0.146 ... 0.273)	-0.086 (-0.49 ... 0.21)	219.676
CNRM-CM5_r1_WRF381P (1)	bad	good	0.277 (0.208 ... 0.326)	-0.14 (-0.68 ... 0.10)	226.606
EC-EARTH_r1_crCLIM-v1-1 (Multiple realisations)	reasonable	good	0.414 (0.285 ... 0.718)	-0.64 (-1.2 ... -0.33)	173.469
EC-EARTH_r1_RACMO22E (Multiple realisations)	good	good	0.348 (0.255 ... 0.414)	-0.096 (-0.45 ... 0.19)	248.004
EC-EARTH_r1_RCA4 (Multiple realisations)	good	reasonable	0.271 (0.206 ... 0.324)	-0.25 (-0.72 ... -0.011)	198.280
EC-EARTH_r12_CCLM4-8-17 (1)	reasonable	good	0.290 (0.217 ... 0.356)	-0.29 (-0.62 ... -0.062)	217.699
EC-EARTH_r12_crCLIM-v1-1 (Multiple realisations)	good	good	0.306 (0.219 ... 0.403)	-0.42 (-1.1 ... -0.19)	194.762
EC-EARTH_r12_HadREM3-GA7-05 (1)	reasonable	good	0.292 (0.227 ... 0.429)	-0.39 (-1.1 ... -0.25)	234.219
EC-EARTH_r12_RACMO22E (Multiple realisations)	good	good	0.279 (0.210 ... 0.378)	-0.48 (-1.1 ... -0.28)	195.593
EC-EARTH_r12_RCA4 (Multiple realisations)	reasonable	reasonable	0.305 (0.221 ... 0.364)	-0.24 (-0.56 ... -0.022)	199.711

https://doi.org/10.25561/104550.

EC-EARTH_r12_RegCM4-6 (1)	bad	reasonable	0.235 (0.168 ... 0.338)	-0.67 (-1.2 ... -0.24)	163.768
EC-EARTH_r12_WRF381P (1)	good	good	0.269 (0.205 ... 0.315)	-0.16 (-0.54 ... 0.018)	178.725
EC-EARTH_r3_crCLIM-v1-1 (Multiple realisations)	good	good	0.328 (0.245 ... 0.391)	-0.15 (-0.53 ... 0.17)	228.631
EC-EARTH_r3_RACMO22E (Multiple realisations)	good	good	0.323 (0.247 ... 0.400)	-0.058 (-0.41 ... 0.26)	224.045
EC-EARTH_r3_RCA4 (Multiple realisations)	reasonable	reasonable	0.345 (0.249 ... 0.420)	-0.090 (-0.33 ... 0.16)	211.408
HadGEM2-ES_r1_ALADIN63 (1)	good	good	0.297 (0.226 ... 0.384)	-0.26 (-1.1 ... -0.067)	294.317
HadGEM2-ES_r1_CCLM4-8-17 (1)	good	good	0.309 (0.239 ... 0.442)	0.051 (-1.1 ... 0.34)	238.595
HadGEM2-ES_r1_crCLIM-v1-1 (1)	good	good	0.391 (0.262 ... 0.487)	-0.14 (-0.49 ... 0.13)	215.362
HadGEM2-ES_r1_HadREM3-GA7-05 (1)	good	good	0.320 (0.242 ... 0.379)	-0.18 (-0.49 ... -0.023)	238.863
HadGEM2-ES_r1_RACMO22E (1)	good	good	0.379 (0.279 ... 0.451)	-0.27 (-0.73 ... 0.028)	226.797
HadGEM2-ES_r1_RCA4 (1)	good	reasonable	0.318 (0.238 ... 0.382)	-0.32 (-0.68 ... -0.070)	203.048
HadGEM2-ES_r1_WRF381P (1)	good	good	0.222 (0.157 ... 0.263)	0.0082 (-0.30 ... 0.29)	233.240
IPSL-CM5A-MR_r1_RACMO22E (1)	bad	reasonable	0.442 (0.340 ... 0.510)	0.15 (-0.22 ... 0.45)	218.746
IPSL-CM5A-MR_r1_RCA4 (1)	bad	reasonable	0.356 (0.265 ... 0.429)	0.052 (-0.22 ... 0.29)	191.010
IPSL-CM5A-MR_r1_REMO2015 (1)	bad	reasonable	0.376 (0.282 ... 0.441)	-0.12 (-0.42 ... 0.065)	137.159
IPSL-CM5A-MR_r1_WRF381P (1)	bad	good	0.210 (0.155 ... 0.251)	-0.12 (-0.54 ... 0.30)	197.744
MPI-ESM-LR_r1_ALADIN63 (1)	good	good	0.289 (0.211 ... 0.358)	-0.30 (-1.0 ... -0.11)	251.139
MPI-ESM-LR_r1_CCLM4-8-17 (1)	good	good	0.250 (0.161 ... 0.339)	-0.18 (-1.1 ... 0.15)	208.414

https://doi.org/10.25561/104550.

MPI-ESM-LR_r1_crCLIM-v1-1 (1)	good	good	0.331 (0.220 ... 0.405)	-0.083 (-0.36 ... 0.28)	258.816
MPI-ESM-LR_r1_HadREM3-GA7-05 (1)	reasonable	good	0.297 (0.234 ... 0.349)	0.032 (-0.43 ... 0.29)	263.209
MPI-ESM-LR_r1_RACMO22E (1)	good	good	0.274 (0.199 ... 0.324)	-0.15 (-0.46 ... 0.11)	208.791
MPI-ESM-LR_r1_RCA4 (Multiple realisations)	good	reasonable	0.278 (0.213 ... 0.355)	-0.30 (-1.1 ... -0.15)	174.015
MPI-ESM-LR_r1_RegCM4-6 (1)	reasonable	reasonable	0.215 (0.161 ... 0.242)	-0.27 (-0.57 ... 0.00074)	0.003
MPI-ESM-LR_r1_REMO2009 (Multiple realisations)	good	good	0.308 (0.232 ... 0.391)	-0.38 (-1.1 ... -0.075)	157.846
MPI-ESM-LR_r1_WRF361H (Multiple realisations)	good	good	0.460 (0.220 ... 0.848)	-0.43 (-1.3 ... 0.28)	197.921
MPI-ESM-LR_r1_WRF381P (1)	good	good	0.345 (0.261 ... 0.502)	-0.39 (-1.1 ... -0.19)	166.317
MPI-ESM-LR_r2_crCLIM-v1-1 (Multiple realisations)	good	good	0.303 (0.176 ... 0.378)	-0.063 (-0.31 ... 0.38)	250.772
MPI-ESM-LR_r2_RCA4 (Multiple realisations)	good	reasonable	0.230 (0.164 ... 0.282)	-0.22 (-0.71 ... 0.032)	159.288
MPI-ESM-LR_r2_REMO2009 (1)	good	good	0.297 (0.227 ... 0.344)	-0.085 (-0.46 ... 0.26)	159.265
MPI-ESM-LR_r3_crCLIM-v1-1 (Multiple realisations)	good	good	0.259 (0.194 ... 0.316)	-0.087 (-0.45 ... 0.11)	245.476
MPI-ESM-LR_r3_RCA4 (Multiple realisations)	good	reasonable	0.233 (0.179 ... 0.284)	-0.055 (-0.69 ... 0.15)	230.536
MPI-ESM-LR_r3_REMO2015 (1)	good	good	0.296 (0.227 ... 0.355)	-0.23 (-0.53 ... -0.0048)	188.199
NorESM1-M_r1_ALADIN63 (1)	good	good	0.350 (0.243 ... 0.437)	-0.28 (-0.67 ... 0.000080)	0.003
NorESM1-M_r1_crCLIM-v1-1 (1)	bad	good	0.364 (0.244 ... 0.462)	-0.15 (-0.41 ... 0.22)	219.456
NorESM1-M_r1_HadREM3-GA7-05 (1)	reasonable	good	0.311 (0.243 ... 0.363)	-0.030 (-0.50 ... 0.23)	226.290
NorESM1-M_r1_RACMO22E (1)	reasonable	good	0.291 (0.215 ... 0.353)	-0.22 (-0.48 ... -0.0068)	214.826

https://doi.org/10.25561/104550.

NorESM1-M_r1_RCA4 (1)	good	reasonable	0.291 (0.207 ... 0.350)	-0.17 (-0.57 ... 0.067)	184.351
NorESM1-M_r1_RegCM4-6 (1)	bad	reasonable	0.268 (0.209 ... 0.295)	-0.11 (-0.39 ... 0.28)	0.003
NorESM1-M_r1_REMO2015 (1)	bad	good	0.286 (0.217 ... 0.338)	-0.078 (-0.48 ... 0.29)	160.779
NorESM1-M_r1_WRF381P (1)	bad	good	0.302 (0.206 ... 0.452)	0.000050 (-1.0 ... 0.00023)	0.002
UKCP18 land-rcm					
UKCP18-01 (1)	good	good	0.293 (0.208 ... 0.379)	-0.066 (-0.57 ... 0.24)	280.338
UKCP18-04 (1)	good	good	0.282 (0.196 ... 0.336)	-0.092 (-0.28 ... 0.16)	244.086
UKCP18-05 (1)	good	good	0.179 (0.126 ... 0.215)	0.0016 (-0.30 ... 0.37)	255.538
UKCP18-06 (1)	good	good	0.307 (0.209 ... 0.381)	-0.16 (-0.48 ... 0.090)	197.596
UKCP18-07 (1)	good	good	0.351 (0.262 ... 0.430)	-0.14 (-0.43 ... 0.091)	326.577
UKCP18-08 (1)	good	good	0.386 (0.263 ... 0.474)	-0.011 (-0.36 ... 0.21)	291.568
UKCP18-09 (1)	good	good	0.254 (0.186 ... 0.305)	-0.30 (-0.66 ... 0.093)	219.171
UKCP18-10 (1)	good	good	0.319 (0.225 ... 0.393)	-0.35 (-0.61 ... -0.14)	212.367
UKCP18-11 (1)	good	good	0.260 (0.190 ... 0.314)	-0.046 (-0.53 ... 0.32)	252.818
UKCP18-12 (1)	good	good	0.337 (0.264 ... 0.387)	0.032 (-0.28 ... 0.47)	289.557
UKCP18-13 (1)	good	good	0.449 (0.340 ... 0.533)	-0.26 (-0.50 ... -0.11)	227.819
UKCP18-15 (1)	good	good	0.407 (0.327 ... 0.467)	-0.046 (-0.36 ... 0.23)	232.645
HighResMIP					
MPI-ESM1-2-HR (1)	reasonable	reasonable	0.459 (0.332 ... 0.561)	-0.24 (-0.58 ... -0.13)	168.250
CMCC-CM2-HR4 (1)	reasonable	bad	0.310 (0.218 ... 0.385)	-0.17 (-0.70 ... 0.24)	134.300
CNRM-CM6-1-HR (1)	reasonable	good	0.381 (0.274 ... 0.457)	-0.17 (-0.49 ... 0.11)	223.360
HadGEM3-GC31-MM (1)	reasonable	good	0.249 (0.187 ... 0.300)	-0.17 (-0.42 ... 0.035)	226.680

https://doi.org/10.25561/104550.

5 Multi-method multi-model attribution

This section shows Probability Ratios and change in intensity ΔI for models and also includes the values calculated from the fits with observations.

Table 2: *Probability Ratio and change in intensity for the models that passed the validation tests, for the ER region.*

Model / Observations	a. Past vs. present		b. Present vs. future	
	Probability ratio PR [-]	**Change in intensity ΔI [%]**	**Probability ratio PR [-]**	**Change in intensity ΔI [%]**
Stations composite	1.4 (0.0043 ... 24)	4.1 (-49 ... 30)		
MSWEP	0.82 (0.0059 ... 18)	-2.9 (-32 ... 40)		
ERA5	0.32 (0.000050 ... 6.2)	-10 (-28 ... 16)		
CNRM-CM5_r1_ALADIN63 (1)	16 (0.82 ... ∞)	15 (-1.7 ... 46)	1.6 (0.0 ... 6.5)	2.8 (-19 ... 16)
CNRM-CM5_r1_ALARO-0 (1)	0.37 (0.14 ... 15)	-7.2 (-21 ... 7.7)	0.87 (0.0 ... 4.5)	-0.87 (-18 ... 14)
EC-EARTH_r12_WRF381P (1)	4.6 (0.41 ... ∞)	6.0 (-7.1 ... 19)	1.0 (0.0 ... 7.3)	0.19 (-17 ... 13)
EC-EARTH_r3_RACMO22E (Multiple realisations)	1.7 (0.22 ... ∞)	4.2 (-24 ... 35)	1.6 (0.038 ... 6.0)	3.3 (-13 ... 18)
HadGEM2-ES_r1_CCLM4-8-17 (1)	3.4 (0.31 ... ∞)	9.9 (-20 ... 54)	2.0 (0.0 ... 8.1)	6.0 (-19 ... 23)
HadGEM2-ES_r1_WRF381P (1)	4.0 (0.49 ... ∞)	12 (-11 ... 35)	0.075 (0.0 ... 1.4)	-16 (-39 ... 3.3)
MPI-ESM-LR_r1_RACMO22E (1)	66 (0.95 ... ∞)	17 (-0.59 ... 36)	1.2 (0.0 ... 5.9)	1.0 (-18 ... 16)
MPI-ESM-LR_r2_crCLIM-v1-1 (Multiple realisations)	4.7 (0.53 ... ∞)	14 (-9.1 ... 40)	0.16 (0.0 ... 1.8)	-13 (-42 ... 5.9)
MPI-ESM-LR_r2_REMO2009 (1)	0.54 (0.17 ... ∞)	-3.9 (-17 ... 14)	0.25 (0.0 ... 2.9)	-5.6 (-20 ... 7.3)
UKCP18-01 (1)	4.2 (0.30 ... ∞)	12 (-26 ... 39)	0.36 (0.0 ... 2.3)	-10 (-45 ... 12)
UKCP18-04 (1)	0.36 (0.12 ... 1.4e+2)	-8.6 (-32 ... 13)	1.8 (0.0046 ... 5.9)	6.0 (-22 ... 24)
UKCP18-05 (1)	0.90 (0.14 ... ∞)	-1.0 (-42 ... 26)	0.80 (0.0 ... 4.1)	-2.1 (-24 ... 24)
UKCP18-06 (1)	0.61 (0.14 ... ∞)	-3.2 (-25 ... 24)	2.7 (0.0 ... 7.8)	8.4 (-23 ... 24)
UKCP18-07 (1)	4.3 (0.26 ... ∞)	9.5 (-20 ... 38)	0.29 (0.0 ... 2.3)	-6.7 (-43 ... 7.8)
UKCP18-08 (1)	0.87 (0.17 ... ∞)	-1.8 (-33 ... 62)	0.44 (0.0 ... 3.7)	-7.6 (-48 ... 18)
UKCP18-09 (1)	1.7 (0.091 ... ∞)	1.5 (-30 ... 16)	4.1 (0.015 ... 11)	14 (-13 ... 31)
UKCP18-10 (1)	0.28 (0.11 ... ∞)	-4.4 (-12 ... 13)	6.7 (0.0 ... 14)	16 (-21 ... 29)
UKCP18-11 (1)	3.2 (0.23 ... ∞)	10 (-33 ... 47)	0.63 (0.0 ... 4.5)	-2.2 (-20 ... 16)
UKCP18-12 (1)	2.9 (0.16 ... ∞)	15 (-58 ... 62)	0.30 (0.0 ... 2.7)	-14 (-44 ... 21)

https://doi.org/10.25561/104550.

6 Hazard synthesis

For the event definition described above we evaluate the influence of anthropogenic climate change by calculating the probability ratio as well as the change in intensity, using observations and climate models. Models which do not pass the evaluation tests described above are excluded from the analysis. The aim is to synthesise results from models that pass the evaluation along with the observations-based products, to give an overarching attribution statement. Figures 7 and 8 show the changes in probability and intensity for the observations (blue) and models (red). To combine them into a synthesised assessment, first, a representation error is added (in quadrature) to the observations, to account for the difference between observation-based datasets that cannot be explained by natural variability. This is shown in these figures as white boxes around the light blue bars. The dark blue bar shows the average over the observation-based products. The dark red bar shows the model average, consisting of a weighted mean using the (uncorrelated) uncertainties due to natural variability. Observation-based products and models are combined into a single result in two ways. Firstly, we neglect common model uncertainties beyond the intermodel spread that is depicted by the model average, and compute the weighted average of models (dark red bar) and observations (dark blue bar): this is indicated by the magenta bar. Because, due to common model uncertainties, model uncertainty can be larger than the intermodel spread, we also show the more conservative estimate of an unweighted direct average of observations (dark red bar) and models (dark blue bar) contributing 50% each, indicated by the white box around the magenta bar in the synthesis figures. Neither observational products nor climate models show a significant change in likelihood or intensity for heavy spring precipitation in the Emilia-Romagna region; this means that the only difference between the weighted and unweighted result is that the latter is centred more firmly on 1.

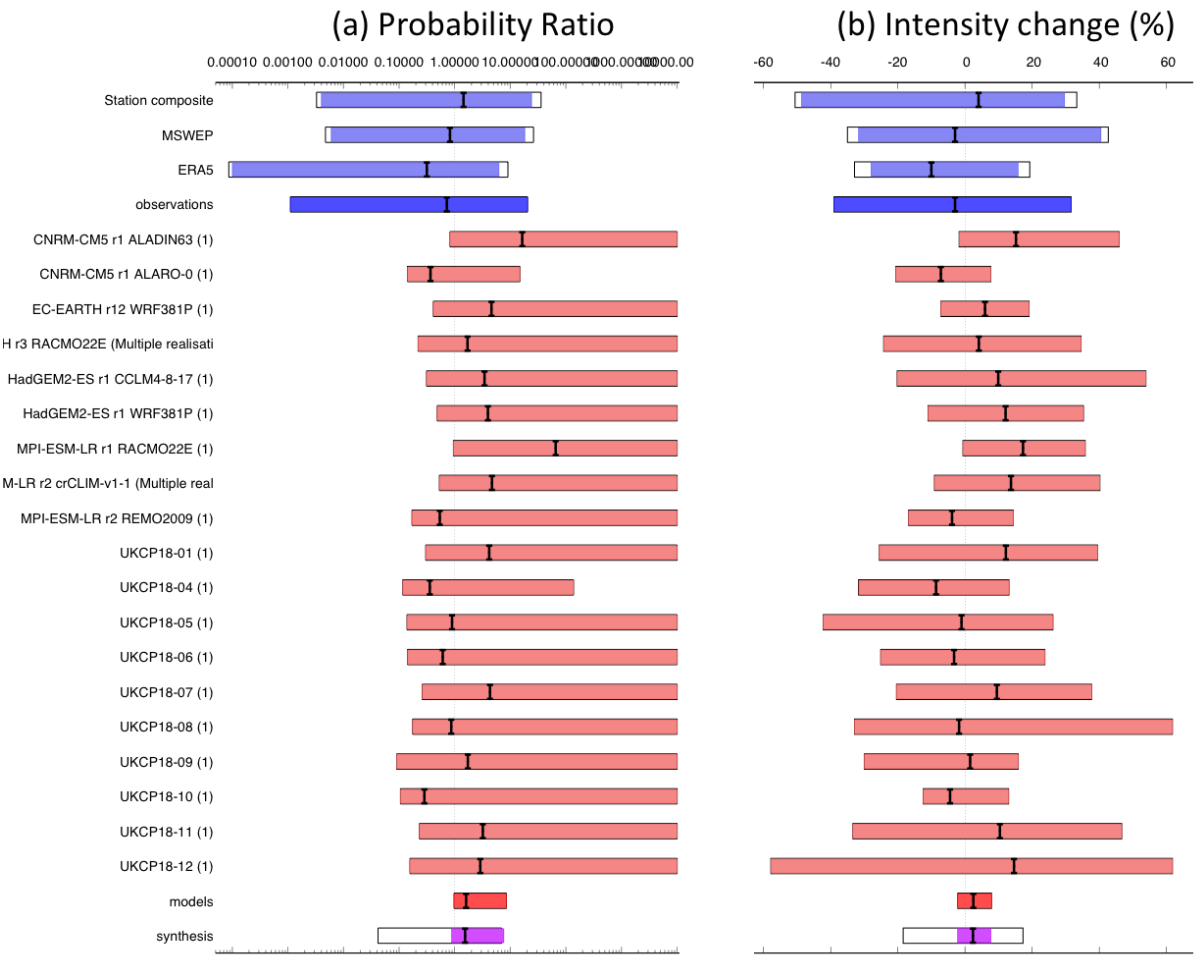

https://doi.org/10.25561/104550.

Figure 7: *Synthesis of (a) probability ratios and (b) intensity changes when comparing the return period and magnitudes of the 2023 AMJ maximum 21-day accumulated rainfall over the ER region in the 2023 climate and a 1.2°C cooler climate.*

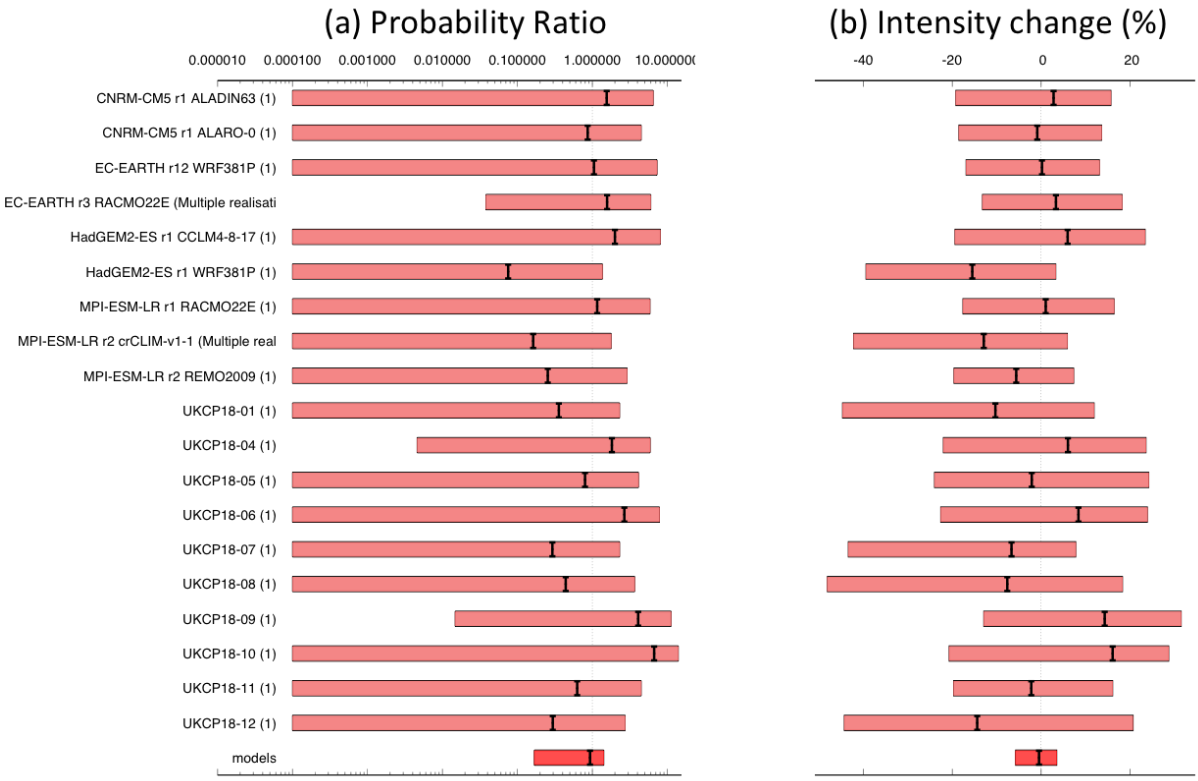

Figure 8: *Synthesis of (a) probability ratios and (b) intensity changes when comparing the return period and magnitudes of the 2023 AMJ maximum 21-day accumulated rainfall over the ER region in the 2023 climate and a 0.8°C warmer climate.*

No single model shows a significant increase or decrease in the likelihood of the event occurring neither with respect to the warming up till now (Figure 7) nor for a further warming of 0.8°C (Figure 8). The synthesis results are in agreement with previous research (see Section 1) indicating a decrease in low pressure systems in this region: this is an example of a region where thermodynamic and dynamic changes in heavy rainfall act in opposite directions, resulting in no overall change in the likelihood or intensity of heavy spring precipitation in the Emilia-Romagna region.

7 Vulnerability & exposure

In addition to the meteorological hazard, it is important to understand the vulnerability and exposure factors that also contributed to the impacts of this event. This section outlines the unique characteristics of the event, and highlights how vulnerable groups were disproportionately impacted. It goes on to discuss factors such as land use and urban planning which may have increased the likelihood of flooding, as well as the flood management system in place.

The devastating impacts experienced from this event did not happen as a result of one rainfall event, but rather a series of heavy rainfall events, the first of which saturated the region's clay soil, causing subsequent rainfall runoff to overflow rivers and triggering landslides throughout the region. According

to a 2021 report from ISPRA, the Italian government's environment agency, an alarming 93.4% of the country's municipalities (7,423 in total) are at risk of landslides, floods, and coastal erosion (ISPRA, 2021). As a result of the landslides and flooding over 15,000 people were displaced from their homes, over 600 roads closed, and at least 16 people were killed (The Guardian, 17 May 2023; ANSA 20 May 2023). It also led to extensive damage to the regionally important agricultural sector, including an estimated 1.5 billion euros of damage estimated from potential root rot resulting from stagnant water (Earth, 2023).

7.1 Flood risk management

Adverse weather conditions all over Italy were forecasted as early as April 2nd, with heavy rainfall, thunderstorm, and strong wind warnings released for North-eastern Italy (yellow category) (Crisis24, 2023a). On April 20th, the Emilia Romagna region was put in the orange category (mid-level in a 3-tier scale), with thunderstorm warnings (Crisis24, 2023b). By May 2nd, the Civil Protection updated the alert from orange to red in the region (Italy24, 2023). The forecasts were accompanied with messages on hazardous conditions that were expected, along with information on potential disruptions to transportation and business.

The Functional Centres located in the Emilia-Romagna region issued bulletins and warnings in which both the evolution of the phenomena and the expected criticality levels on the territory were reported (CPD, 2023). Based on these, early warnings were widely issued through mass media (newspapers, news channels and television).

In Italy, the municipal operational centres and the regional operations rooms are responsible for local level flood risk management, while the National Civil Protection Service is overall responsible for coordinating disaster management responses in the country (CPD, 2023). In 2021, the Emilia-Romagna region revised and adopted the second cycle of its Flood Management plan (FMP), which includes planning, preparedness and programming components. Programmes under the FMP include soil and coast protection interventions, basin planning and interventions against hydrogeological instability (Geoportale Nazionale, 2023).

Closures of road networks along embankments started on May 2nd, due to the overflowing of the Sillaro river. This preceded the bulk of flooding to come, and evacuation activities had also been initiated in Faenza, Castel Bolognese and Conselice. Within the first week of flooding, the government promptly declared a state of emergency that will last 12 months and has allocated 10 million euros for the most urgent interventions in agreement with the Region (ANSA, 2023). The government has swiftly collaborated with the region to ensure the safety and smooth evacuation of families at risk from flooding, landslides, and damage to road infrastructure, public and private buildings, hydraulic defence works, and the network of essential services (ANSA, 2023).

7.2 Land use and urban planning

Land use has a significant effect on the severity and impacts of riverine and flash flooding - different types of soil cover affect surface runoff, infiltration rates, and flow speeds differently, and also expose assets and contribute to the overall damage. Recent changes in land-use in the region include significant increases in built-up areas, especially since the 1960s, with urban areas expanding over agricultural land (Pistocchi et al. 2015).

https://doi.org/10.25561/104550.

Emilia-Romagna is a highly urbanised, wealthy, and developed region (OECD, 2022). Bologna is its main metropolitan centre, surrounded by a highly integrated network of small and medium-sized cities and towns. The floods affected over 100 cities and towns in the region, affecting the urban centres of Forlì, Cesena, Rimini, Conselice, Ponticelli, Bagnacavallo, Riccione, Faenza, Lugo, Russi, and others. At the time of writing, many towns are still under water.

The region consists of various housing types, including converted historic buildings, apartments, villas, and rural dwellings. The cities in Emilia-Romagna generally have well-preserved historic centres, characterised by compact layouts, narrow streets, and buildings dating back centuries. Neighbourhoods range from well-preserved historic centres to residential areas with a mix of housing options. Furthermore, Emilia-Romagna also has a strong industrial base, characterised by the presence of a number of micro and small firms located in industrial districts (Bianchi & Bianchi, 2019).

Urban planning plays an important role in either exacerbating or mitigating flood risk. In recent decades, rapid urbanisation and increasingly dense urban fabric has limited space for water drainage and so increased the risk of flooding (Pistocchi et al., 2015). As cities grow and expand, it will be necessary to restrict development in flood-prone areas to reduce the vulnerability and potential damage caused by flooding. Urban planners should develop appropriate zoning regulations and building codes that restrict development in flood-prone areas, ensuring that new construction is located in safer zones. In addition, it has been identified that the drainage network must be retrofitted if significantly higher costs from flooding are to be avoided (Pistocchi et al., 2015).

Various policies and projects have been put in place to increase urban green spaces across Emilia-Romagna (Grigoletto et al. 2021), which can significantly mitigate flooding risk (Jongman, 2018). In 2020, a project to increase green areas by 20% in cities in Emilia-Romagna was approved (Grigoletto et al. 2021). The region also allocated a range of resources to promote sustainable development, protect and enhance the natural environment as well as the environmental heritage throughout the whole region (ibid.).

7.3 Intersecting vulnerabilities

Among all exposed populations to flooding, certain groups are particularly vulnerable to the impacts of these shocks for intersecting reasons. Groups vulnerable to flooding and associated landslides tend to include the elderly, children, and people living with some form of disability, as they often have limited mobility and depend on others for support (see e.g. Chisty et al., 2021; Chakraborty et al., 2019; Houston et al., 2020). According to news reports, the majority of those deceased in the deluges in May were indeed elderly individuals who died in their private homes; some of whom were bedridden, others reportedly reluctant to evacuate (Rai News, 2023). A study conducted on quantifying social vulnerability to floods in the region in 2017 assessed the Emilia-Romagna region to have medium social vulnerability to flood impacts (Roder et al. 2017). The study metric included factors such as age, economic/employment status, family structure, dependency on land, gender, special needs, etc.

Socioeconomic vulnerabilities known to drive flood risk in Northern Italy notably include poor housing conditions - often in locations with high exposure - as well as low economic status, commonly rendering immigrants and ethnic minorities such as Roma and Sinti communities disproportionately vulnerable

(Di Giustino et al., 2022; Roder et al., 2017). This is in part linked to discrimination faced in the private housing and job markets (OHCHR, 2021).

Finally, occupational vulnerability was demonstrated by the vast impacts on the agricultural sector, withover 5,000 agri-businesses submerged and the sector at large suffering approximately 300 million euros in damages (Carboni, 2023). Providing a salient case of intersectional vulnerability, it is important to note that roughly one-third of people employed in the agricultural sector in Italy are estimated to be migrants and refugees (Info Migrants, 2022).

7.4 V&E conclusions

The rarity of this event (a 1-in-200 year event) implies that it could not be expected that existing infrastructure be built to withstand such extreme rainfall. The finding that during the spring season, this type of event is not occurring more frequently, further complicates calls for adaptation within the region to this type of event. Adaptation decisions should be based on a holistic review of how the climate has already changed in the region, and future projections of changes. However, there are 'low regret' adaptation options that could be beneficial for this region because they have co-benefits for multiple hazards (e.g. floods, droughts, heat), as well as improving the wellbeing of the general public and biodiversity. For example, increasing the 'sponginess' of cities with the help of water and vegetation based nature-based solutions can offer multiple co-benefits: (i) a holistic, multi-hazard approach to reducing risk including for flooding and landslides, heatwaves, and drought (Kumar et al., 2020); (ii) addressing risks that come with increasing urbanisation such as urban heat island effects (Hayes et al., 2022); and (iii) improving the overall wellbeing of residents by enabling nature-based experiences and reducing stress (Coventry et al., 2021; Shanahan et al., 2019; Kolokotsa et al., 2020). Further, a number of social security measures could be adopted to reduce the economic impacts of flooding (or other extreme weather events) on affected families. This could be in the form of (i) reduction, partial/full waiver of contributions to pension or unemployment funds for workers in the affected regions; (ii) waiver of school fees for children in the affected regions as long as the state of national emergency lasts; (iii) needs-based psychosocial support and counselling for post-disaster trauma, either through online sessions or municipal health care units. While psychosocial support has already been made available, its continuation beyond the immediate shock could improve long-term wellbeing (Regione Emilia-Romagna, 2023). Such initiatives can support recovery, contribute to well-being, and enable transitioning to normalcy, for flood events like these as well as other hazards in the future.

Finally, natural flood risk management of various types (i.e. increasing forest cover, re-meandering streams, re-creating wetlands, etc.) can all have the effect of slowing down river flows, decreasing flash flood risk, and creating stronger ecosystem regulators areas; all in all, decrease flood impacts on both arable and urban areas. With many parts of Europe seeing increasing severe drought risk, various methods to store the water from these floods (e.g. in constructed wetlands, slower rivers, irrigation systems, etc.) could increase the resilience of agricultural systems in the region, particularly as the summer months begin and forecasted El Niño conditions point to hotter, drier seasons over Europe. This would require further research but has already been pointed to as a tool (see e.g. Ward et al., 2020).

Data availability

Time series used in this study are available via the Climate Explorer.

References

All references are given as hyperlinks in the text.

Please cite this report as:

Barnes, C; Faranda, D; Coppola, E; Grazzini, F; Zachariah, M; Lu, C; Kimutai, J; Pinto, I; Pereira, CM; Sengupta, S; Vahlberg, M; Singh, R; Heinrich, D; Otto, FEL (2023). Limited net role for climate change in heavy spring rainfall in Emilia-Romagna.
DOI: https://doi.org/10.25561/104550